Perturbation theory of nonlinear, non-self-adjoint eigenvalue problems: simple eigenvalues

Georg A. Mensah[a,b], Alessandro Orchini[b], Jonas P. Moeck[c]

[a] *CAPS Laboratory, Department of Mechanical and Process Engineering, ETH Zürich, Switzerland*
[b] *Institut für Strömungsmecahnik und Technische Akustik, TU Berlin, Germany*
[c] *Department of Mechanical and Process Engineering, NTNU Trondheim, Norway*

Abstract

The study of the vibrational modes and stability of a given physical system has strong bounds with the efficient numerical evaluation of its eigenvalues. The operators governing the eigenproblem are, in general, nonlinear in the eigenvalue and non-self-adjoint, which makes the repeated solution of the eigenvalue problem (necessary for example when the effect of several parameter values on the system needs to be assessed) expensive. This study reviews the adjoint-based incremental procedure for calculating the coefficients of power series expansion of simple (non-degenerate) eigenvalues and their eigenvectors. These expansions approximate the eigenvalues to any desired order in a finite region. An efficient numerical implementation of the theory is proposed, and it is shown how high-order power series approximations of the eigenvalues give very accurate results within the radius of convergence of the power series, which is finite and generally not small. Furthermore, the domain of convergence of the power series might be extended by considering Padé expansions of the eigenvalues. Examples involving the stability of the Orr–Sommerfeld equation, the biharmonic equation for the vibrational modes of a membrane, and the emission of sounds from a Rijke tube because of thermoacoustic feedback are used to assess and validate the theory.

Keywords: high-order perturbation theory, adjoints, eigenvalue problems

1. Introduction

Eigenvalue problems are of fundamental importance in science and engineering. They are often associated with wave phenomena, arising, for ex-

ample, from the Schrödinger equation in quantum mechanics, or from the Helmholtz equation in acoustics. Other classic examples of eigenvalue problems are those that appear in the linear stability analysis of the equations governing various physical phenomena. A more comprehensive list of research fields in which eigenvalue problems commonly appear can be found in [1, 2]. Due to the abundant appearance of eigenvalue problems, and the fact that these are rarely treatable analytically, efficient algorithms for their solution are needed. When considering eigenvalue problems subject to parameter variations over a certain range, a considerable computational effort may be necessary. Solving the eigenvalue problem once may already be computationally demanding – this is especially true for eigenvalue problems that depend nonlinearly on the eigenvalue. Solving the eigenproblem multiple times for different values of the parameter of interest is even more challenging, and is often a poor strategy. Instead, using a perturbation approach, aided by adjoint-based methods, can significantly speed up the computations.

The eigenvalue problems considered in this study involve linear operator families $\mathcal{L}(z)$ which may depend nonlinearly on $z \in \mathbb{C}$. [1] The problem is phrased as follows: given an operator family $\mathcal{L}(z)$, find $\lambda \in \mathbb{C}$ and a corresponding function $v \neq 0$ such that

$$\mathcal{L}(\lambda)v = 0. \tag{1}$$

The elements of the pair (λ, v) that solve the above eigenproblem are called eigenvalue and eigenfunction, respectively. Equation (1) may also refer to boundary value problems defined on a domain Ω. They can be written as

$$\mathcal{L}(\lambda)v := \begin{cases} \mathcal{L}_\Omega(\lambda)v = 0 & \text{in } \Omega \\ \mathcal{L}_{\partial\Omega}(\lambda)v = 0 & \text{on } \partial\Omega \end{cases} . \tag{2}$$

The operator family $\mathcal{L}(z)$ is called self-adjoint if $\mathcal{L}^\dagger(z) = \mathcal{L}(\overline{z})$; it is called normal if $\mathcal{L}\mathcal{L}^\dagger = \mathcal{L}^\dagger\mathcal{L}$; and it is called non-normal otherwise ($\mathcal{L}^\dagger$ denotes the adjoint operator of $\mathcal{L}$, defined in §2). In this study, no assumption is made regarding the normality of the operator $\mathcal{L}(z)$, meaning that the presented theory is applicable to all of these classes of operators. Furthermore, the eigenvalue problem associated with $\mathcal{L}(z)$ will be called linear if $\mathcal{L}(z) = (\mathcal{A} + z\mathcal{B})$, the classic eigenvalue problem, and nonlinear if $\mathcal{L}$ depends on z in a

[1] As for the examples given below, for problems arising in practical engineering the operator $\mathcal{L}$ is a mapping of an Hilbert space onto itself.

nonlinear fashion, for example if the operator is polynomial in z or depends exponentially on it.

From an operator theory viewpoint, eigenvalues are complex-valued numbers λ at which the family of linear operators $\mathcal{L}(z)$ possesses no inverse [3]. Throughout this paper it is assumed that $\mathcal{L}(z)$ is analytic in z in some neighborhood around an eigenvalue λ. Moreover the discussion is limited to discretizations $\mathbf{L}(z)$ of $\mathcal{L}(z)$, which is assumed to be bounded. The set of all eigenvalues of a discretized operator family is called the spectrum of the discretized operator family. Except for trivial cases where the operator family is non-invertible for any z, the spectrum of a discretized operator family is discrete, i.e., it consists of isolated points in the complex plane. An eigenvalue is classified depending on its algebraic and geometric multiplicity [3]. Eigenvalues with equal algebraic and geometric multiplicity are referred to as semi-simple. This includes simple eigenvalues, which have algebraic and geometric multiplicity equal to 1. Eigenvalues with an algebraic multiplicity greater than one are referred to as degenerate. Degenerate eigenvalues that are not semi-simple are called defective – their algebraic multiplicity is greater than their geometric multiplicity. Although the spectrum of $\mathbf{L}(z)$ may contain degenerate eigenvalues, the present study will only consider the expansion around simple eigenvalues.

In addition to obtaining a specific solution of an eigenvalue problem, it is often of interest to understand how the solution (eigenvalue and/or eigenvector) varies when some parameters governing the operator $\mathcal{L}$ are changed. The parameter changes could be related to a comparison of several designs in engineering applications, or to the evaluation of uncertainties in the modeling parameters, particularly in stability analysis. ε represents a generic parameter of interest that may affect any component of the problem – for example the structure of the operator, the boundary conditions, or the shape of the considered domain. By explicitly accounting for the dependence of the operator on the parameter, the (discretized) eigenvalue problem (1) reads[2]

$$\mathbf{L}(\lambda, \varepsilon)\boldsymbol{v} = \mathbf{0}. \tag{3}$$

Except for very simple cases, closed-form solutions to the parameter-

[2]Note that different symbols are used for continuous operators, $\mathcal{L}$, and their finite-dimensional discretization matrices, $\mathbf{L}$. The same holds true for the eigenfunctions, v, which are approximated by the eigenvectors, $\boldsymbol{v}$. To ease the notation, however, λ indicates an eigenvalue in both the continuous and discrete formulations.

dependent eigenvalue problem (3) do not exist; however, an eigensolution may be known for a specific value of the parameter ε. This is referred to as the unperturbed solution. Without loss of generality, the unperturbed solution can be assumed to correspond to $\varepsilon = 0$, and the corresponding eigenpair is denoted with λ_0 and $\boldsymbol{v}_0$ so that $\mathbf{L}(\lambda_0, 0)\boldsymbol{v}_0 = \mathbf{0}$. One can then exploit the knowledge on the unperturbed solution and estimate the solutions for values of $\varepsilon \neq 0$ by approximating the eigenvalues and eigenfunctions of the perturbed problem with truncated power series. The stipulated power series ansätze read

$$\lambda(\varepsilon) = \lambda_0 + \sum_{n=1}^{\infty} \lambda_n \varepsilon^n \qquad \text{and} \qquad \boldsymbol{v}(\varepsilon) = \boldsymbol{v}_0 + \sum_{n=1}^{\infty} \boldsymbol{v}_n \varepsilon^n \tag{4}$$

for the eigenvalue and eigenfunction, respectively. This type of approximation and the machinery used to calculate the power series coefficients is known as Rayleigh–Schrödinger perturbation theory, as it was first employed by Lord Rayleigh to solve models of vibrating strings [4] and by Schrödinger to compute spectral absorption lines of the hydrogen atom subjected to the Stark effect [5].

Schrödinger considered problems arising from quantum mechanics, which are typically self-adjoint and linear in the eigenvalue λ. Furthermore, he only considered perturbations of the operator that are linear in the parameter ε, explicitly derived first-order equations, and sketched how the approach can be generalized to arbitrary order. Soon after, the method was generalized by Fues [6] to account for a nonlinear dependence of the operator on the parameter ε; his work contains the equations for large-order eigenvalue and eigenvector corrections of self-adjoint operators that depend linearly on the eigenvalue. The method can also be extended to generalized eigenvalue problems, as in [7]. Nowadays, perturbation theory of linear, self-adjoint eigenvalue problems has become a well established mathematical tool, and is extensively treated in [8]. Multi-paramneter approximation theory for linear self-adjoint eigenvalue problems can be, e.g., found in [9]. Focusing on simple eigenvalues, which are those investigated in this study, explicit formulas for the eigenvalue and eigenvector corrections up to 4th order arising from non-normal operators that are linear in both the eigenvalue and the perturbation parameter were given in [10]. In fluid mechanics, the use of non-self-adjoint perturbation theory for the investigation of the influence of base-flow modifications on the eigenvalues of the (non-normal) Navier–Stokes equation was

proposed by [11], and applied by [12] at first order for the cylinder flow, and by [13] at second order for a wake flow. [14] contains a detailed explanation of how this can be achieved numerically even for operators discretized by very large matrices. In more recent years, the use of adjoint-based perturbation theory has been quite successful in the field of thermoacoustics, which involves the study of non-normal eigenvalue problems that are nonlinear in both the eigenvalue and the perturbation parameter. This was introduced in [15] for first-order sensitivities only, and generalized to higher orders in [16]. The theory for nonlinear eigenvalue problems is significantly younger and not nearly as far developed as for linear problems. General reviews on nonlinear eigenvalue problems are [17, 18]. [19] demonstrated how to derive arbitrary order sensitivity equations for simple eigenvalues utilizing both the corresponding adjoint and direct eigenvectors. In our study, this theory is presented for completeness, and is derived using a more explicit notation which is more suitable for an efficient numerical implementation of the perturbation theory at high orders. An alternative algorithm using no adjoint eigenvectors is presented in [20]. Some theorems on the existence and convergence of large-order polynomial expansions for semi-simple eigenvalues can be found in [21], and aspects of defective eigenvalues are discussed in [22]. Chapters 7 and 11 in [23] give a comprehensive literature review and a modern introduction to the perturbation theory of non-self-adjoint boundary eigenvalue problems.

When first introduced, performing large-order perturbation calculations was a tedious task, as it requires the evaluation of several derivatives and the combination of numerous terms, whose number grows exponentially with perturbation order. With the advancements in computer technology this has become considerably easier. Algebraically perturbing (undiscretized) differential equations to large orders with computer algebra systems is nowadays a standard technique in theoretical physics, see e.g. [24]. Indeed, computers and numerical methods have become so powerful that accurately solving the eigenvalue problem (2) by means of, e.g., high-dimensional finite-element discretization methods is feasible, although it remains numerically demanding.

For large problem sizes, with nonlinear dependence of $\mathbf{L}$ on λ, solving (3) may require considerable computational effort. In this context, Rayleigh–Schrödinger perturbation theory plays a key role. By performing *once* the calculations of the coefficients for a high-order power series expansion of the solutions of (3), one can then accurately estimate the eigenvalues and eigenfunctions for *any* value of the perturbation parameter ε within a certain range

(the convergence radius of the power series). This range can be considerably extended by using rational polynomial approximations. Several applications of this concept are found in the literature, and include computation and continuation of dispersion curves (e.g., for photonic crystals [25]), sensitivity analysis (e.g., in flow control [13]), or Monte Carlo-free uncertainty quantification of stability analysis results (e.g., in thermoacoustics [26]).

This study focuses on adjoint-based high-order perturbation theory of simple eigenvalues. The theory in its most general form is presented. It contains all the formulas needed for calculating at an arbitrary order the coefficients for the power series expansions of simple eigenvalues and corresponding eigenvectors of nonlinear eigenvalue problems. The procedure is analogous to that outlined in [19], but it is more explicit and uses a notation that can be straightforwardly coded. This allows us to efficiently implement the theory in a framework that is independent from a particular physical problem, and can accurately estimate eigenvalue and eigenvector corrections to very high orders. Using these corrections, accurate predictions on the dependence of the eigenvalues on a parameter can be made within the radius of convergence of the power series. In addition, we also utilize Padé approximants – i.e, rational polynomials – to overcome the limit imposed by the radius of convergence of the power series, which is a standard method for series acceleration [24, 27].

The manuscript is organized as follows: in §2 a detailed derivation of the large-order equations is presented and discussed; it is followed by a discussion on how these concepts are efficiently implemented into a numerical framework in §3. Three test cases, chosen from eigenvalue problems arising in the fields of fluid mechanics, §4.1, structural mechanics, §4.2, and thermoacoustics, §4.3, are subsequently used to exemplify the theory with practical emphasis on vibrational problems. We also demonstrate that the rate of convergence of the eigenvalues greatly increases when the functional ansatz is changed from a power series to a Padé series. Finally, a summary of the study and some concluding remarks close the study in §5.

2. Theory

To find the coefficients of the power series ansätze, eqs. (4) are substituted into the eigenvalue problem (3):

$$\mathsf{L}\left(\lambda_0 + \sum_{n=1}^{\infty} \lambda_n \varepsilon^n, \varepsilon\right)\left(\boldsymbol{v}_0 + \sum_{n=1}^{\infty} \boldsymbol{v}_n \varepsilon^n\right) = \mathbf{0}. \tag{5}$$

It is assumed that L is analytic in both z and ε in some neighborhood of the unperturbed solution λ_0 for $\varepsilon = 0$. By truncating the power series at the desired order of approximation N, the operator $\mathsf{L}(z, \varepsilon)$ can be expanded into the bi-variate power series

$$\mathsf{L}(\lambda_0 + \Delta z, \varepsilon) \approx \sum_{n=0}^{N} \varepsilon^n \sum_{m=0}^{N} (\Delta z)^m \mathsf{L}_{m,n}. \tag{6}$$

The $\approx$ symbol emphasizes that, by truncating the series, we introduce an error of order $\mathcal{O}\left(\varepsilon^{N+1}\right)$, using the big O notation in the $\varepsilon \to 0$ limit. This notation will be adopted throughout the article, whenever the equations contain truncated power series. Moreover, $\mathsf{L}_{m,n}$ are the Taylor-series coefficients defined by

$$\mathsf{L}_{m,n} := \frac{1}{m!n!} \frac{\partial^{m+n} \mathsf{L}}{\partial z^m \partial \varepsilon^n}\bigg|_{\substack{z=\lambda_0 \\ \varepsilon=0}}. \tag{7}$$

Introducing (6) into (5), defining $\Delta\lambda := \sum_{n=1}^{N} \lambda_n \varepsilon^n = \Delta z$, leads to

$$\left[\sum_{n=0}^{N} \varepsilon^n \sum_{m=0}^{N} (\Delta\lambda)^m \mathsf{L}_{m,n}\right]\left[\sum_{n=0}^{N} \boldsymbol{v}_n \varepsilon^n\right] \approx \mathbf{0}. \tag{8}$$

Introducing the multi-index $\boldsymbol{\mu} := [\mu_1, \mu_2, \ldots, \mu_N]$, the tuple $\boldsymbol{\lambda} := [\lambda_1, \lambda_2, \ldots, \lambda_N]$, and exploiting the multinomial theorem yields

$$(\Delta\lambda)^m = \left(\sum_{n=1}^{N} \lambda_n \varepsilon^n\right)^m = \sum_{|\boldsymbol{\mu}|=m} \binom{m}{\boldsymbol{\mu}} \prod_{n=1}^{N} (\lambda_n \varepsilon^n)^{\mu_n} = \sum_{|\boldsymbol{\mu}|=m} \binom{m}{\boldsymbol{\mu}} \boldsymbol{\lambda}^{\boldsymbol{\mu}} \varepsilon^{|\boldsymbol{\mu}|_{\mathrm{w}}}. \tag{9}$$

By definition, the entries of the multi-index $\boldsymbol{\mu}$ are non-negative integers, $\mu_i \in \mathbb{N}$. Moreover, the following standard definitions and properties of multi-indices hold:

$$|\boldsymbol{\mu}| := \sum_{n=1}^{N} \mu_n, \qquad \binom{|\boldsymbol{\mu}|}{\boldsymbol{\mu}} := \frac{|\boldsymbol{\mu}|!}{\prod_{n=1}^{N} (\mu_n!)}, \qquad \boldsymbol{\lambda}^{\boldsymbol{\mu}} := \prod_{n=1}^{N} \lambda_n^{\mu_n}. \tag{10}$$

Additionally, $|\boldsymbol{\mu}|_{\mathrm{w}}$ denotes a weighted sum of the multi-indices:

$$|\boldsymbol{\mu}|_{\mathrm{w}} := \sum_{n=1}^{N} n\mu_n. \tag{11}$$

Plugging (9) back into (8) yields

$$\sum_{n=0}^{N} \sum_{m=0}^{N} \sum_{|\boldsymbol{\mu}|=m} \sum_{l=0}^{N} \varepsilon^{n+|\boldsymbol{\mu}|_{\mathrm{w}}+l} \binom{m}{\boldsymbol{\mu}} \boldsymbol{\lambda}^{\boldsymbol{\mu}} \mathbf{L}_{m,n} \boldsymbol{v}_l \approx \mathbf{0}. \tag{12}$$

In order to sort for like powers of ε, the substitution $k = n + |\boldsymbol{\mu}|_{\mathrm{w}} + l$ is made. This eventually yields

$$\sum_{k=0}^{N} \varepsilon^k \sum_{m=0}^{k} \sum_{|\boldsymbol{\mu}|_{\mathrm{w}}=m} \sum_{n=0}^{k-|\boldsymbol{\mu}|_{\mathrm{w}}} \binom{|\boldsymbol{\mu}|}{\boldsymbol{\mu}} \boldsymbol{\lambda}^{\boldsymbol{\mu}} \mathbf{L}_{|\boldsymbol{\mu}|,n} \boldsymbol{v}_{k-n-|\boldsymbol{\mu}|_{\mathrm{w}}} \approx \mathbf{0}. \tag{13}$$

In the last step, the summation limits have been changed to account only for powers of ε up to order N. Indeed, eq. (12) contains terms of order $\mathcal{O}\left(\varepsilon^{N+1}\right)$ and higher. These terms are irrelevant for the calculation of the power series coefficients up to the desired order N, and are neglected in the following. In particular, because in (13) the index l cannot be negative, one has $l = k - n - |\boldsymbol{\mu}|_{\mathrm{w}} \geq 0$. Thus, the sum over n is limited to $k - |\boldsymbol{\mu}|_{\mathrm{w}}$. The set of multi-indices on which the third summation is performed has also changed from $|\boldsymbol{\mu}|$ to $|\boldsymbol{\mu}|_{\mathrm{w}}$, in order to guarantee that $k - |\boldsymbol{\mu}|_{\mathrm{w}} \geq 0$. From their definitions, it is clear that the weighted sum $|\boldsymbol{\mu}|_{\mathrm{w}}$ is greater or equal than $|\boldsymbol{\mu}|$, therefore the set of multi-indices having $|\boldsymbol{\mu}|_{\mathrm{w}} \leq k$ is a subset of those having $|\boldsymbol{\mu}| \leq k$. It is only this specific subset contributing to the relevant powers of ε.

Lastly, the second and third summations can be merged, yielding

$$\sum_{k=0}^{N} \varepsilon^k \sum_{0 \leq |\boldsymbol{\mu}|_{\mathrm{w}} \leq k} \sum_{n=0}^{k-|\boldsymbol{\mu}|_{\mathrm{w}}} \binom{|\boldsymbol{\mu}|}{\boldsymbol{\mu}} \boldsymbol{\lambda}^{\boldsymbol{\mu}} \mathbf{L}_{|\boldsymbol{\mu}|,n} \boldsymbol{v}_{k-n-|\boldsymbol{\mu}|_{\mathrm{w}}} \approx \mathbf{0}, \tag{14}$$

where $\sum_{0 \leq |\boldsymbol{\mu}|_{\mathrm{w}} \leq k}$ denotes the sum over all multi-indices having a weighted sum greater than or equal to 0 but less than or equal to k. One can show that such a list of multi-indices has a strong connection with the problem of identifying all the partitions of integer numbers, as it will be further discussed in §3.

From eq. (14), the equation that needs to be solved at each order $k \leq N$ can be identified:

$$\sum_{0 \leq |\boldsymbol{\mu}|_{\mathrm{w}} \leq k} \sum_{n=0}^{k-|\boldsymbol{\mu}|_{\mathrm{w}}} \binom{|\boldsymbol{\mu}|}{\boldsymbol{\mu}} \boldsymbol{\lambda}^{\boldsymbol{\mu}} \mathbf{L}_{|\boldsymbol{\mu}|,n} \boldsymbol{v}_{k-n-|\boldsymbol{\mu}|_{\mathrm{w}}} = \mathbf{0}. \tag{15}$$

In deriving explicit formulas for the solution of a generic order k, it is convenient to rewrite (15) as

$$\mathbf{L}_{0,0} \boldsymbol{v}_k = -\boldsymbol{r}_k - \lambda_k \mathbf{L}_{1,0} \boldsymbol{v}_0, \tag{16}$$

where

$$\boldsymbol{r}_k := \sum_{n=1}^{k} \mathbf{L}_{0,n} \boldsymbol{v}_{k-n} + \sum_{\substack{0 < |\boldsymbol{\mu}|_{\mathrm{w}} \leq k \\ \boldsymbol{\mu} \neq \mathbf{1}_k}} \sum_{n=0}^{k-|\boldsymbol{\mu}|_{\mathrm{w}}} \binom{|\boldsymbol{\mu}|}{\boldsymbol{\mu}} \boldsymbol{\lambda}^{\boldsymbol{\mu}} \mathbf{L}_{|\boldsymbol{\mu}|,n} \boldsymbol{v}_{k-n-|\boldsymbol{\mu}|_{\mathrm{w}}}. \tag{17}$$

Here the sum over the multi-indices excludes the multi-index

$$\mathbf{1}_k := [\overbrace{0, \ldots, 0, 1}^{k \text{ terms}}, 0, \ldots, 0], \tag{18}$$

as this is the only term containing λ_k, and it is explicitly accounted for in eq. (16). This definition of $\boldsymbol{r}_k$ will be convenient in §2.1.

Given a baseline solution $\mathbf{L}_{0,0} \boldsymbol{v}_0 = \mathbf{0}$, eq. (16) provides a set of linear, non-homogeneous equations that need to be solved in ascending order for $1 \leq k \leq N$. For example, the baseline problem and the equations for the

first and second order are:

$$\mathcal{O}\left(\varepsilon^0\right): \qquad \mathbf{L}_{0,0}\boldsymbol{v}_0 = \mathbf{0}, \tag{19a}$$

$$\mathcal{O}\left(\varepsilon^1\right): \qquad \mathbf{L}_{0,0}\boldsymbol{v}_1 = -\mathbf{L}_{0,1}\boldsymbol{v}_0 - \lambda_1\mathbf{L}_{1,0}\boldsymbol{v}_0, \tag{19b}$$

$$\mathcal{O}\left(\varepsilon^2\right): \qquad \mathbf{L}_{0,0}\boldsymbol{v}_2 = -(\mathbf{L}_{0,1} + \lambda_1\mathbf{L}_{1,0})\boldsymbol{v}_1 - (\mathbf{L}_{0,2} + \lambda_1\mathbf{L}_{1,1} + \lambda_1^2\mathbf{L}_{2,0})\boldsymbol{v}_0 - \lambda_2\mathbf{L}_{1,0}\boldsymbol{v}_0. \tag{19c}$$

2.1. Incremental scheme for the calculation of power series coefficients

The term $\boldsymbol{r}_k$ in eq. (16) depends on coefficients λ_n and $\boldsymbol{v}_n$ of orders less than k. Because these coefficients have already been calculated at lower orders, the only remaining unknowns in eq. (16) are λ_k and $\boldsymbol{v}_k$. However, $\mathbf{L}_{0,0}$ is not invertible because $\mathbf{L}_{0,0}\boldsymbol{v}_0 = \mathbf{0}$. Hence, some conditions need to be imposed on eq. (16) to guarantee its solvability. These conditions are known as Fredholm alternatives, and they guarantee the existence of the solution, i.e., of the unknowns λ_k and $\boldsymbol{v}_k$ [28, Chap. 9]. Because the matrix $\mathbf{L}_{0,0}$ is generally non-self-adjoint, the calculation of the adjoint eigensolution $\boldsymbol{v}_0^\dagger$ of the unperturbed problem is required for the formulation of the solvability condition.

The adjoint eigenvector $\boldsymbol{v}_0^\dagger$ is defined as the eigenvector of the adjoint operator corresponding to the same eigenvalue λ_0:

$$\mathbf{L}_{0,0}^\dagger\boldsymbol{v}_0^\dagger = \mathbf{0}. \tag{20}$$

Given an inner product $\langle\cdot|\cdot\rangle$, the adjoint $\mathbf{L}_{0,0}^\dagger$ of $\mathbf{L}_{0,0}$ is defined by

$$\langle\mathbf{L}_{0,0}^\dagger\boldsymbol{g}|\boldsymbol{f}\rangle = \langle\boldsymbol{g}|\mathbf{L}_{0,0}\boldsymbol{f}\rangle, \tag{21}$$

which needs to hold for arbitrary vectors $\boldsymbol{f}$ and $\boldsymbol{g}$. In particular, by choosing as a test vector $\boldsymbol{g}$ the adjoint eigenvector $\boldsymbol{v}_0^\dagger$, one has

$$\langle\boldsymbol{v}_0^\dagger|\mathbf{L}_{0,0}\boldsymbol{f}\rangle \overset{(21)}{=} \langle\mathbf{L}_{0,0}^\dagger\boldsymbol{v}_0^\dagger|\boldsymbol{f}\rangle \overset{(20)}{=} \langle\mathbf{0}|\boldsymbol{f}\rangle = 0. \tag{22}$$

Since $\boldsymbol{f}$ is an arbitrary vector, $\mathbf{L}_{0,0}\boldsymbol{f}$ is an arbitrary element in the range of $\mathbf{L}_{0,0}$. Therefore, eq. (22) proves that the range of $\mathbf{L}_{0,0}$ is orthogonal to the adjoint eigenspace. Because (16) admits a solution if and only if its r.h.s.

is in the range of $\mathbf{L}_{0,0}$, the following solvability condition – the Fredholm alternative – must be satisfied[3]:

$$\left\langle \boldsymbol{v}_0^\dagger \middle| \boldsymbol{r}_k + \lambda_k \mathbf{L}_{1,0} \boldsymbol{v}_0 \right\rangle = 0. \tag{23}$$

For the case of a simple eigenvalue there is only one Fredholm condition, and (23) effectively defines the eigenvalue expansion coefficient at order k:

$$\lambda_k := -\frac{\left\langle \boldsymbol{v}_0^\dagger \middle| \boldsymbol{r}_k \right\rangle}{\left\langle \boldsymbol{v}_0^\dagger \middle| \mathbf{L}_{1,0} \boldsymbol{v}_0 \right\rangle}. \tag{24}$$

Substituting λ_k into (16) guarantees that a solution for the eigenvector $\boldsymbol{v}_k$ exists, and can be expressed in terms of the generalized inverse $\mathbf{L}_{0,0}^g$ of $\mathbf{L}_{0,0}$ as:

$$\boldsymbol{v}_k = -\mathbf{L}_{0,0}^g \left[\boldsymbol{r}_k - \frac{\left\langle \boldsymbol{v}_0^\dagger \middle| \boldsymbol{r}_k \right\rangle}{\left\langle \boldsymbol{v}_0^\dagger \middle| \mathbf{L}_{1,0} v_0 \right\rangle} \mathbf{L}_{1,0} \boldsymbol{v}_0 \right] + c_k \boldsymbol{v}_0 := \boldsymbol{v}_k^\perp + c_k \boldsymbol{v}_0. \tag{25}$$

The solution to eq. (16), $\boldsymbol{v}_k$, is not unique as there is the freedom to add an arbitrary (complex-valued) multiple c_k of eigenvector $\boldsymbol{v}_0$ of the unperturbed operator. This is because $\boldsymbol{v}_0$ belongs to the nullspace of $\mathbf{L}_{0,0}$. To that effect, $\boldsymbol{v}_k^\perp$ in (25) denotes the component of $\boldsymbol{v}_k$ that is orthogonal to $\boldsymbol{v}_0$, i.e., $\left\langle \boldsymbol{v}_k^\perp \middle| \boldsymbol{v}_0 \right\rangle = 0$. $\boldsymbol{v}_k^\perp$ is furthermore the minimum-norm solution to eq. (16), and it will be convenient in §2.2, where it is shown that imposing a normalization condition on the perturbed eigenvectors removes the ambiguity on the constant c_k.

Note that solving the above equations requires knowledge of *only* the direct and adjoint eigenvectors corresponding to the simple eigenvalue of interest. In contrast, classical Rayleigh–Schrödinger perturbation theory, as often presented in the literature (e.g. [24]) for linear self-adjoint problems, requires knowledge of all eigenvalues and eigenfunctions of the unperturbed matrix family $\mathbf{L}(z, 0)$. The latter is necessary because the eigenvector corrections $\boldsymbol{v}_k$ can be expressed as a linear combination of a complete basis. For self-adjoint, linear eigenvalue problems, the set of eigenvectors – which

[3]This holds true for bounded operators, and is sufficient for the scope of this study because, for any numerical application, one deals with a discretized, finite-dimensional matrix representation of the operators.

are orthogonal to each other – is chosen as basis for the considered vector space. Although generalizable to non-Hermitian, nonlinear eigenvalue problems, this approach has the drawback that the eigenvector series may converge slowly to the desired eigenvector correction terms. Furthermore, for discretizations represented by large matrices, it is numerically demanding to calculate a large set of eigenfunctions of the unperturbed operator. Hence, even for self-adjoint, linear eigenvalue problems, the correction terms are nowadays obtained by directly solving eq. (16) using the described adjoint-based solution approach [19, 29, 28].

The equations presented in this section give rise to an incremental procedure: starting with the knowledge of a simple eigenvalue λ_0 of $\mathbf{L}(z, \varepsilon = 0)$, its direct eigenvector $\boldsymbol{v}_0$ and its adjoint eigenvector $\boldsymbol{v}_0^\dagger$, one can compute the power series coefficients λ_n and $\boldsymbol{v}_n$ order by order, by solving the set of linear equations (24) and (25). This allows for accurately estimating the eigenvalues and eigenvectors of the eigenproblem for values of $\varepsilon \neq 0$. This procedure is straightforward to implement in a numerical algorithm, but particular care needs to be taken for efficiently evaluating $\boldsymbol{r}_k$ – which contains a very large number of terms at high orders, eq. (17) – as will be discussed in §3.

2.2. Eigenvector normalization

The eigenvector corrections $\boldsymbol{v}_k$ as defined in (25) are not uniquely determined because $\boldsymbol{v}_0$ lies in the kernel of $\mathbf{L}_{0,0}$. Hence, if $\boldsymbol{v}_k$ is a solution of (16), so is $\boldsymbol{v}_k + c_k \boldsymbol{v}_0$, where c_k is an arbitrary constant. Ultimately, this ambiguity of the eigenvector correction arises because eigenvectors can be arbitrarily scaled. Imposing a normalization condition to the eigenvectors removes this ambiguity and determines the eigenvector corrections $\boldsymbol{v}_k$ uniquely. This section presents two methods that can be used for determining the normalization coefficients: an *a priori* method in §2.2.1, which can be solved order by order together with the equations for the eigenvalues and the eigenvectors; an *a posteriori* method in §2.2.2, to be performed after the calculation of the power series coefficients.

2.2.1. A priori normalization

Without loss of generality, a normalization condition can be imposed that requires the norm of the perturbed eigenvectors to be unity, i.e. $\|\boldsymbol{v}(\varepsilon)\|^2 = \big\langle \boldsymbol{v}(\varepsilon) \big| \boldsymbol{v}(\varepsilon) \big\rangle = 1$ for any value of ε. Expanding the expression for $\boldsymbol{v}(\varepsilon)$ us-

ing (4) and collecting the terms for powers of ε up to N yields

$$\left\langle \sum_{k=0}^{N} \varepsilon^k \boldsymbol{v}_k \middle| \sum_{k=0}^{N} \varepsilon^k \boldsymbol{v}_k \right\rangle \approx \sum_{k=0}^{N} \varepsilon^k \sum_{j=0}^{k} \langle \boldsymbol{v}_{k-j} | \boldsymbol{v}_k \rangle = 1, \tag{26}$$

which implies

$$\langle \boldsymbol{v}_0 | \boldsymbol{v}_0 \rangle = 1 \qquad \text{and} \qquad \sum_{j=0}^{k} \langle \boldsymbol{v}_{k-j} | \boldsymbol{v}_j \rangle = 0 \quad \text{for } k = 1, 2, \ldots, N. \tag{27}$$

Because the scalar product is generally defined over the field of complex numbers $\mathbb{C}$, the normalization condition (26) still leaves freedom on a global phase factor on $\boldsymbol{v}(\varepsilon)$. It is convenient to choose this phase such that the projection of the perturbed eigenvector on the unperturbed one is a real-valued number:

$$\operatorname{Im}\left[\langle \boldsymbol{v}_0 | \boldsymbol{v}(\varepsilon) \rangle\right] = 0. \tag{28}$$

Power series expansion yields

$$\begin{aligned} &\operatorname{Im}\left[\langle \boldsymbol{v}_0 | \boldsymbol{v}(\varepsilon) \rangle\right] = \operatorname{Im}\left[\left(1 + \sum_{k=1}^{N} \varepsilon^k \langle \boldsymbol{v}_0 | \boldsymbol{v}_k \rangle\right)\right] = 0 \\ \Leftrightarrow \quad &\operatorname{Im}\left[\langle \boldsymbol{v}_0 | \boldsymbol{v}_k \rangle\right] = 0 \quad \forall k \in [1, N]. \end{aligned} \tag{29}$$

Combining this with the anti-linearity of the scalar product yields

$$\operatorname{Im}\left[\langle \boldsymbol{v}_0 | \boldsymbol{v}_n \rangle\right] = \operatorname{Im}\left[\overline{\langle \boldsymbol{v}_n | \boldsymbol{v}_0 \rangle}\right] = 0 \quad \Leftrightarrow \quad \langle \boldsymbol{v}_0 | \boldsymbol{v}_n \rangle = \langle \boldsymbol{v}_n | \boldsymbol{v}_0 \rangle \in \mathbb{R}, \tag{30}$$

where the overbar denotes complex conjugation. This can be used for obtaining an explicit formula for the coefficients c_k. From (27) follows

$$\langle \boldsymbol{v}_k | \boldsymbol{v}_0 \rangle + \langle \boldsymbol{v}_0 | \boldsymbol{v}_k \rangle + \sum_{j=1}^{k-1} \langle \boldsymbol{v}_{k-j} | \boldsymbol{v}_j \rangle = 0, \tag{31}$$

where the first and last term were pulled out from the sum. Using eqs. (25) and (30) results in

$$\langle \boldsymbol{v}_0 | \boldsymbol{v}_k \rangle = \langle \boldsymbol{v}_0 | \boldsymbol{v}_k^{\perp} + c_k \boldsymbol{v}_0 \rangle = \underbrace{\langle \boldsymbol{v}_0 | \boldsymbol{v}_k^{\perp} \rangle}_{=0} + c_k \underbrace{\langle \boldsymbol{v}_0 | \boldsymbol{v}_0 \rangle}_{=1} = c_k = -\frac{1}{2} \sum_{j=1}^{k-1} \langle \boldsymbol{v}_{k-j} | \boldsymbol{v}_j \rangle. \tag{32}$$

The right hand side in the above equation only depends on eigenfunction corrections of order lower than k. This allows computing c_k explicitly order by order, in an incremental fashion like the computation of λ_k. A general result is that, regardless of the problem under investigation, $c_1 = 0$, which is a common condition that can be found in the literature for first order approximations [29, 28].

2.2.2. A posteriori normalization

Because the normalization coefficients do not affect the calculation of the eigenvalue and eigenvector corrections, they can be calculated in a post-processing step for any ε of interest. Indeed, their calculation is not necessary if the analysis concerns only the eigenvalues. From the power series expansion follows

$$\boldsymbol{v}(\varepsilon) \approx \boldsymbol{v}_0 + \sum_{k=1}^{N} (\boldsymbol{v}_k^{\perp} + c_k \boldsymbol{v}_0)\varepsilon^k = \underbrace{\left(\sum_{k=1}^{N} c_k \varepsilon^k\right)}_{:=c(\varepsilon)} \boldsymbol{v}_0 + \underbrace{\left(\boldsymbol{v}_0 + \sum_{k=1}^{N} \varepsilon^k \boldsymbol{v}_k^{\perp}\right)}_{:=\boldsymbol{v}^*(\varepsilon)}. \quad (33)$$

In this equation, $c(\varepsilon)$ is the unknown factor of vectors $\boldsymbol{v}_0$ to be added to $\boldsymbol{v}^*(\varepsilon)$ to have the best estimate of the perturbed eigenvector $\boldsymbol{v}(\varepsilon)$. When this is achieved, the perturbed eigenvalue problem (3) is satisfied so that

$$\mathsf{L}\left(\sum_{k=0}^{N} \lambda_k \varepsilon^k, \varepsilon\right) (\boldsymbol{v}^*(\varepsilon) + c(\varepsilon)\boldsymbol{v}_0) \approx \boldsymbol{0}. \quad (34)$$

In order to ease the notation, the following variables are introduced:

$$\boldsymbol{a} := \mathsf{L}\left(\sum_{k=0}^{N} \lambda_k \varepsilon^k, \varepsilon\right) \boldsymbol{v}^*(\varepsilon), \qquad \boldsymbol{b} := \mathsf{L}\left(\sum_{k=0}^{N} \lambda_k \varepsilon^k, \varepsilon\right) \boldsymbol{v}_0. \quad (35)$$

Decomposing the vector $\boldsymbol{a}$ into components parallel and orthogonal to $\boldsymbol{b}$ yields

$$\boldsymbol{a} = \boldsymbol{a}_{\parallel} + \boldsymbol{a}_{\perp} = \frac{\langle \boldsymbol{a} | \boldsymbol{b} \rangle}{\langle \boldsymbol{b} | \boldsymbol{b} \rangle} \boldsymbol{b} + \boldsymbol{a}_{\perp}. \quad (36)$$

Substitution in (34) yields

$$\left(\frac{\langle \boldsymbol{a} | \boldsymbol{b} \rangle}{\langle \boldsymbol{b} | \boldsymbol{b} \rangle} + c(\varepsilon)\right) \boldsymbol{b} + \boldsymbol{a}_{\perp} \approx \boldsymbol{0}. \quad (37)$$

For this equation to hold, the component $\boldsymbol{a}_\perp$ needs to vanish – this is easy to see in the asymptotic limit $\varepsilon \to 0$ – whereas for the component parallel to $\boldsymbol{b}$ to vanish, it is necessary that

$$c(\varepsilon) = -\frac{\langle \boldsymbol{a} | \boldsymbol{b} \rangle}{\langle \boldsymbol{b} | \boldsymbol{b} \rangle}. \tag{38}$$

Although the *a posteriori* procedure avoids the incremental normalization scheme and, thus, slightly reduces the effect of round-off errors, it has higher computational costs because a different value for $c(\varepsilon)$ has to be computed for each ε of interest. In §4 both types of normalization schemes are applied to test cases, and it is shown that they lead to similar approximation accuracies for the eigenvectors.

3. Discussion on numerical implementation

Details on the numerical implementation of the theory are discussed in this section. The source code used to produce all the results shown in §4 is freely available online[4].

3.1. Continuous vs discrete adjoints

A different representation $\mathbf{L}^\dagger$ of the adjoint operator $\mathcal{L}^\dagger$ is obtained depending on whether the adjoint operator is first derived from the governing equations and then discretized or vice versa. The former is commonly referred to as continuous adjoint, and the latter as discrete adjoint [30]. Throughout the present study, the discrete adjoint is considered, because of two reasons:

(i) when using the standard inner product[5] $\langle \boldsymbol{y} | \boldsymbol{x} \rangle = \boldsymbol{y}^{\mathrm{H}} \boldsymbol{x} = \sum_i \overline{y_i} x_i$, the discrete adjoint of an operator is simply the Hermitian transpose of its matrix representation, $\mathbf{L}^\dagger = \mathbf{L}^{\mathrm{H}}$, which is straightforward to compute. Moreover, direct and adjoint eigenvectors become then equivalent to right and (conjugate transpose of) left eigenvectors of $\mathbf{L}$, and can be automatically computed by means of standard linear-algebra software packages;

[4] https://bitbucket.org/pyholtzdevelopers/public

[5] Note that, although this choice of the inner product is convenient, apart from the normalization of the eigenvector the results of the perturbation theory are inner-product independent.

(ii) in a discrete adjoint formulation, it is guaranteed that the direct and the adjoint operators feature exactly the same eigenvalues (by construction). In a continuous formulation, instead, the eigenvalues of $\mathbf{L}$ and $\mathbf{L}^\dagger$ can be slightly different – depending on how the chosen discretization acts on the structure of the continuous direct and continuous adjoint operators [31]. From a numerical viewpoint, this is not fully consistent because the results can be biased by which eigenvalue – direct or adjoint – is chosen to perform the analysis with.

3.2. Data structuring

In order to efficiently implement the perturbation theory, an appropriate data structure representing the considered nonlinear eigenvalue problem is required. It is convenient to express the matrix families as

$$\mathbf{L}(z,\varepsilon) = \sum_i f_i(z,\varepsilon)\mathbf{M}_i, \tag{39}$$

where f_i are scalar functions in z and ε and $\mathbf{M}_i$ are constant matrices. A major advantage of this representation is that it allows to compute the matrices $\mathbf{L}_{m,n}$ as

$$\mathbf{L}_{m,n} := \frac{1}{n!m!}\frac{\partial^{m+n}}{\partial z^m \partial \varepsilon^n}\mathbf{L}(\lambda,0) = \frac{1}{n!m!}\sum_i \frac{\partial^{m+n}}{\partial z^m \partial \varepsilon^n} f_i(\lambda,0)\mathbf{M}_i. \tag{40}$$

This avoids the error induced by numerical differentiation schemes. Moreover, when performing power series expansions at high orders, it is convenient to build a library providing the functions $f_i(z,\varepsilon)$ together with their derivatives for use at runtime rather than evaluating the derivatives symbolically at runtime. Note that the implementation of the collection of nonlinear eigenvalue problems given in [1] uses a similar data structure for all non-polynomial and non-rational eigenvalue problems. The decomposition (39) is not unique, and leaves some room for optimal implementation, which is generally problem dependent. A strategy that is always possible is to associate each matrix entry with an individual coefficient function f_i. Provided that there is a library containing all these functions, it would suffice to store pointers to these very functions. The memory requirement to store these pointers is comparable to the one needed for storing one dense matrix of floating point numbers. However, many problems feature a number of functions f_i much lower than the total number of matrix entries. In these cases,

a factorization of the terms proportional to the functions f_i naturally arises from the problem statement. This latter strategy is exploited in all the examples given in §4. In any case, because the terms of the summation can be individually evaluated, the data structure has a high potential for parallelization. Also note that the operators $\mathbf{M}_i$ can be represented in a matrix-free fashion, providing only a function that returns the result of the represented matrix–vector multiplications.

3.3. Obtaining a baseline solution

For the perturbation theory to yield accurate predictions for the eigenvalues and eigenvectors as functions of the parameter, it is mandatory to first calculate a high-precision baseline solution – viz., both the eigenvalue, and direct and adjoint eigenvectors. The present study uses a modified version of the generalized Rayleigh quotient iteration [32]. The scheme is a Newton-type iteration on the linear eigenvalue problem

$$\mathbf{L}(\lambda, \varepsilon = 0)\boldsymbol{v} = \xi \boldsymbol{v}, \tag{41}$$

where λ (the eigenvalue of interest) is treated as a parameter, and ξ is a dummy variable representing the eigenvalues of the matrix $\mathbf{L}(\lambda, 0)$. The idea is to find for which values of λ the linear eigenproblem (41) has an eigenvalue $\xi = 0$. Because for these eigenvalues the right hand side vanishes, these $\lambda = \lambda_0$ and their corresponding $v = v_0$ are solutions of (3) at $\varepsilon = 0$.

Equation (41) is a linear eigenvalue problem in ξ. It can be solved by means of standard eigenvalue solvers, perturbation theory, and Newton's method as follows. Starting from an initial guess $\lambda^{\{0\}}$, the direct and adjoint eigenvalue problems for ξ are solved – note that only the eigenvalue ξ with minimum magnitude is of interest. One can then compute the sensitivity $\lambda' := \frac{\mathrm{d}\xi}{\mathrm{d}\lambda}$, and update the guess for $\lambda^{\{1\}} \leftarrow \xi - \frac{\lambda^{\{0\}}}{\lambda'}$. The sensitivity can be obtained using standard perturbation theory for linear eigenvalue problems. For this study, Newton's method has been replaced by a third-order Householder method [33]. This extension of the method requires third-order perturbation theory – as presented in this article – and results in a faster convergence of the iterative algorithm. By iterating this procedure until a desired tolerance is achieved, ξ is steered towards 0, and a solution for the eigenvalue problem (3) is obtained. The recent review [18] provides more details on generalized Rayleigh quotient iteration and a general discussion on methods for the solution of nonlinear eigenvalue problems. A benefit of

this iterative method is that, by prescribing a strict stopping tolerance, it allows computing the baseline eigenvalue at a predefined accuracy.

Note that, the described procedure is a local technique, that usually finds eigensolutions close to the initial guess. An initial guess may be found from a contour-integration-based method see e.g. [34, 18] for a mathematical presentation of such techniques or [35] for a practical application to a thermo-acoustic configuration.

3.4. Numerical implementation of the perturbation theory

Algorithm 1 is an efficient implementation of the perturbation theory with a priori normalization outlined in the previous section. Note that, although $\mathbf{L}_{0,0}$ is rank-deficient with $\boldsymbol{v}_0$ spanning its kernel, the linear system $\mathbf{L}_{0,0}\boldsymbol{x} = \boldsymbol{y}$ admits a solution as $\boldsymbol{y}$ fulfills the solvability condition. However, the solution is not unique, as outlined in §2.2. In order to guarantee uniqueness at this stage, the function $\boldsymbol{x} \leftarrow \textsc{solve}(\mathbf{L}_{0,0}, \boldsymbol{y})$ is assumed to return the minimum-norm solution of $\mathbf{L}_{0,0}\boldsymbol{x} = \boldsymbol{y}$. Computing this solution may be efficiently achieved using a LU-factorization of $\mathbf{L}_{0,0}$ and appropriate projection operations to reduce the norm of $\boldsymbol{y}$. Because the system matrix $\mathbf{L}_{0,0}$ appears at every perturbation order, its LU-factorization is only to be computed once. At no stage it is necessary to build the complete generalized inverse of $\mathbf{L}_{0,0}$.

Note that any vector norm might be used in Algorithm 1. However, the adjoint eigenvector $\boldsymbol{v}_0^\dagger$ fed to the algorithm must be consistently defined with respect to this norm. Commonly, the norm will be induced from the discretization of the considered problem, amounting to $\langle \boldsymbol{a} | \boldsymbol{b} \rangle = \boldsymbol{a}^{\mathrm{H}} \mathbf{Y} \boldsymbol{b}$ where $\mathbf{Y}$ is some symmetric positive-definite matrix. In the simplest case $\mathbf{Y}$ is the identity matrix $\mathbf{I}$ and the norm reduces to the standard norm. Because, the eigenvalue coefficients are independent of the norm, the algorithm may be implemented using the standard norm and the corresponding adjoint eigenvector in line 16 in order to save matrix-vector multiplications, while using a different norm for the normalizations starting in line 18.

The multi-indices necessary to generate $\boldsymbol{r}_k$ are read from file rather than computed at run time. Importantly, the multi-indeces are problem-independent so that they can be built *once* – up to the order of interest – and re-used whenever necessary. Although reading the multi-indices from a file requires more memory usage, the computation is nonetheless significantly accelerated at large perturbation orders. Also, the steps necessary to compute $\boldsymbol{r}_k$ are loop-independent, and the loop can be parallelized, which is crucial for very high-order applications.

Algorithm 1 Factorized implementation of the perturbation theory with a priori normalization

function PERTURB($\mathsf{L}_{m,n}, \boldsymbol{v}_0, \boldsymbol{v}_0^\dagger, N$)

  for $k \leftarrow 1, \ldots, N$ **do**
    $\boldsymbol{r}_k \leftarrow 0$
    for $m \leftarrow 0, \ldots, k$ **do** ▷ parallelizable loops
      for $n \leftarrow 0, \ldots, k-m$ **do**
        if (m,n)=(0,0) **then**
          continue ▷ the term carrying $\mathsf{L}_{0,0}$ is not part of $\boldsymbol{r}_k$
        end if
        $\boldsymbol{w} \leftarrow 0$
        for $\boldsymbol{\mu} \in \{\boldsymbol{\mu} : |\boldsymbol{\mu}| = m, |\boldsymbol{\mu}|_\mathrm{w} \leq k\} \setminus \{\mathbf{1}_k\}$ **do** ▷ read this set from prepared file
          $\boldsymbol{w} \leftarrow \boldsymbol{w} + \boldsymbol{v}_{k-n-|\boldsymbol{\mu}|_\mathrm{w}} \boldsymbol{\lambda}^{\boldsymbol{\mu}} \binom{m}{\boldsymbol{\mu}}$
        end for
        $\boldsymbol{r}_k \leftarrow \boldsymbol{r}_k + \mathsf{L}_{m,n} \boldsymbol{w}$
      end for
    end for

    $\lambda_k \leftarrow -\dfrac{\left\langle \boldsymbol{v}_0^\dagger \middle| \boldsymbol{r}_k \right\rangle}{\left\langle \boldsymbol{v}_0^\dagger \middle| \mathsf{L}_{1,0} \boldsymbol{v}_0 \right\rangle}$
    $\boldsymbol{v}_k^\perp \leftarrow$SOLVE($\mathsf{L}_{0,0}, -\boldsymbol{r}_k - \lambda_k \mathsf{L}_{1,0} \boldsymbol{v}_0$) ▷ is solvable due to solvability condition

    $c_k \leftarrow 0$ ▷ a priori normalization
    for $l \leftarrow 1, \ldots, k-1$ **do**
      $c_k \leftarrow c_k - \frac{1}{2} \left\langle \boldsymbol{v}_l \middle| \boldsymbol{v}_{k-l} \right\rangle$
    end for
    $\boldsymbol{v}_k \leftarrow \boldsymbol{v}_k^\perp + c_k \boldsymbol{v}_0$
  end for

  return $[\lambda_1, \ldots, \lambda_N], [\boldsymbol{v}_1, \ldots, \boldsymbol{v}_N]$
end function

Generating the table of the multi-indeces exploits a connection to number theory, which was reported in [36] for the case of linear eigenvalue problems.

In order to calculate $\boldsymbol{r}_k$ as defined in (17) it is necessary to sum over all multi-indices in the set $\mathbb{M}_l := \{\boldsymbol{\mu} \,|\, |\boldsymbol{\mu}|_\mathrm{w} = l\}$. From the definition of $|\boldsymbol{\mu}|_\mathrm{w}$, and because the elements of the multi-index $\boldsymbol{\mu}$ are integers, it follows

$$|\boldsymbol{\mu}|_\mathrm{w} = \sum_{k=1}^{N} \mu_k k = \sum_{k=1}^{N} \sum_{n=1}^{\mu_k} k = l. \tag{42}$$

This equation shows that the set $\mathbb{M}_l$ is equivalent to all the possible decompositions of the integer l into a sum of integers k. In number theory such a decomposition is called a partition of l. Thus, finding all multi-indices featuring $|\boldsymbol{\mu}|_\mathrm{w} = l$ is equivalent to finding all possible partitions for a given integer l. The accelerated ascending composition generation algorithm (AccelAsc) proposed in [37] has been used to efficiently generate a sequence of all the partitions of a given integer.

3.5. Reduction of matrix-vector multiplications

The interpretation of the multi-indices as partitions of integers is also useful for the analysis of the computational complexity of the algorithm. Let us denote with $p(l)$ the partition function, which returns the number of possible partitions of l. The number of terms in the power series expansion of the eigenvalue problem (14) is

$$\begin{aligned} \text{number of terms } &= \sum_{k=0}^{N} \sum_{0 \le |\boldsymbol{\mu}|_\mathrm{w} \le k} \sum_{n=0}^{k-|\boldsymbol{\mu}|_\mathrm{w}} 1 = \sum_{k=0}^{N} \sum_{m=0}^{k} \sum_{|\boldsymbol{\mu}|_\mathrm{w}=m} \sum_{n=0}^{k-m} 1 \\ &= \sum_{k=0}^{N} \sum_{m=0}^{k} p(m)(k-m+1). \end{aligned} \tag{43}$$

The number of terms of the Nth-order equation is shown in Fig. 1. It increases quickly with N, and its asymptotic behavior is about two orders of magnitude larger than that of the partition function. The computationally most expensive operation in each of these terms is the matrix–vector multiplication $\mathsf{L}_{|\boldsymbol{\mu}|,n} \boldsymbol{v}_{k-n-|\boldsymbol{\mu}|_\mathrm{w}}$. It is, therefore, desirable to minimize the number of these operations. Because the same operator $\mathsf{L}_{|\boldsymbol{\mu}|,n}$ acts on several vectors, factorizing these matrices saves a significant number of matrix–vector

multiplications. From eq. (14), simple index manipulation yields

$$\sum_{k=0}^{N} \varepsilon^k \sum_{m=0}^{k} \sum_{n=0}^{k-m} \mathsf{L}_{m,n} \underbrace{\sum_{\substack{|\boldsymbol{\mu}|=m \\ |\boldsymbol{\mu}|_{\mathrm{w}} \le k}} \binom{m}{\boldsymbol{\mu}} \boldsymbol{\lambda}^{\boldsymbol{\mu}} \boldsymbol{v}_{k-n-|\boldsymbol{\mu}|_{\mathrm{w}}}}_{:=\boldsymbol{w}_{m,n}}, \tag{44}$$

where the last sum runs over the set of all multi-indices with $|\boldsymbol{\mu}| = m$ and $|\boldsymbol{\mu}|_{\mathrm{w}} \le k$. Thus, by first calculating the vectors $\boldsymbol{w}_{m,n}$ defined in (44) and then performing the operations $\mathsf{L}_{m,n}\boldsymbol{w}_{m,n}$, the total number of matrix-vector multiplications becomes polynomial:

$$\begin{aligned} \text{number of matrix–vector multiplications} &= \sum_{k=0}^{N} \sum_{m=0}^{k} \sum_{n=0}^{k-m} 1 \\ &= \frac{1}{6}N^3 + N^2 + \frac{11}{6}N + 1. \end{aligned} \tag{45}$$

Figure 1 compares the numerical effort arising from a brute-force implementation of eq. (14) with that resulting from an optimal rearrangement of the terms, as in (44) and implemented in Algorithm 1. Already at moderate values of the expansion order N, the two quantities differ by several orders of magnitude.

Further improvement of the algorithm is possible when dealing with eigenvalue problems that are polynomial in the eigenvalue and the parameter, which is common in many applications. Indeed, in these cases all matrices $\mathsf{L}_{m,n}$ with m or n greater than the polynomial order of the eigenvalue or of the parameter, respectively, trivially vanish. As an example, Fig. 1 shows how the number of matrix–vector multiplications reduces for problems that are linear in both the eigenvalue and the parameter.

4. Application examples

This section exemplifies the theory discussed in §2 on the basis of three problems of physical relevance. The perturbation theory results will be compared with eigenvalues and eigenvectors obtained solving the nonlinear eigenvalue problem for several values of the perturbation parameter ε, using the generalized Rayleigh quotient iteration outlined in §3.3. The results of the discussed examples can be reproduced from the publicly available source-code[4].

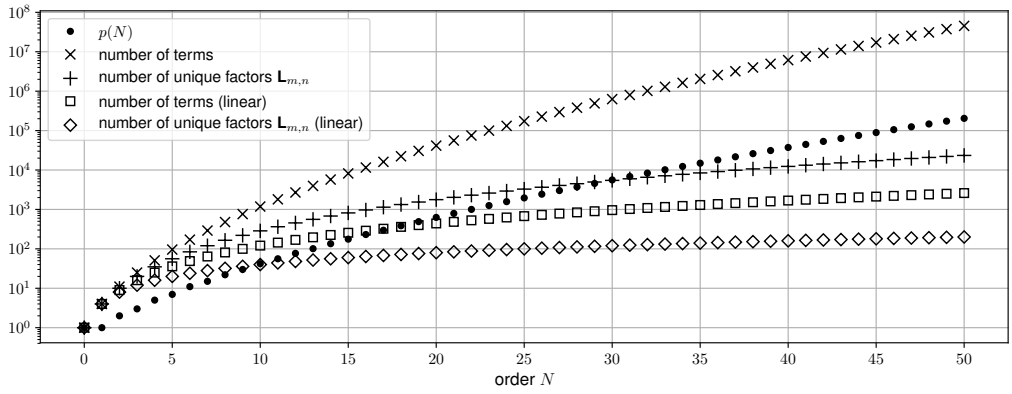

Figure 1: Number of terms and the number of unique factors $\mathbf{L}_{m,n}$ necessary to form $\boldsymbol{r}_k$ for (i) a generic dependence of $\mathbf{L}(z,\varepsilon)$ on its parameters z and ε and (ii) the special case of a linear dependence. The behavior of the partition function is shown for reference. The number of matrix-vector multiplications required by a brute-force algorithm is equivalent to the number of terms, while it reduces to the number of unique factors $\mathbf{L}_{m,n}$ when using Algorithm 1. The number of vector-vector additions required is equal to the number of terms and identical for a brute-force implementation and Algorithm 1.

4.1. Orr–Sommerfeld equation

As a first example, the Orr–Sommerfeld equations are considered. These equations are obtained from a linearization of the Navier–Stokes equations in two dimensions, using the ansatz $f(x,y,t) = v(y)e^{\mathrm{i}(\lambda x - \omega t)}$. They serve as a model for the modal stability of parallel viscous flows. When unstable, structures known as Tollmien-Schlichting waves arise, which can be observed in channel and boundary layer flows [38, 39, 40]. The equation for a channel flow reads

$$\left[\left(\frac{\mathrm{d}^2}{\mathrm{d}y^2} - \lambda^2\right)^2 - \mathrm{iRe}\left((\lambda U - \omega)\left(\frac{\mathrm{d}^2}{\mathrm{d}y^2} - \lambda^2\right) - \lambda U''\right)\right] v = 0. \tag{46}$$

The x-coordinate points into the flow direction, while the y-direction is set perpendicular to it. In this example, plane Couette flow is considered, with walls at $y = \pm 1$. The laminar base velocity profile is parabolic, $U = 1 - y^2$. Re denotes the Reynolds number. No-slip boundary conditions must be satisfied by the mode v at the walls:

$$v(\pm 1) = v'(\pm 1) = 0. \tag{47}$$

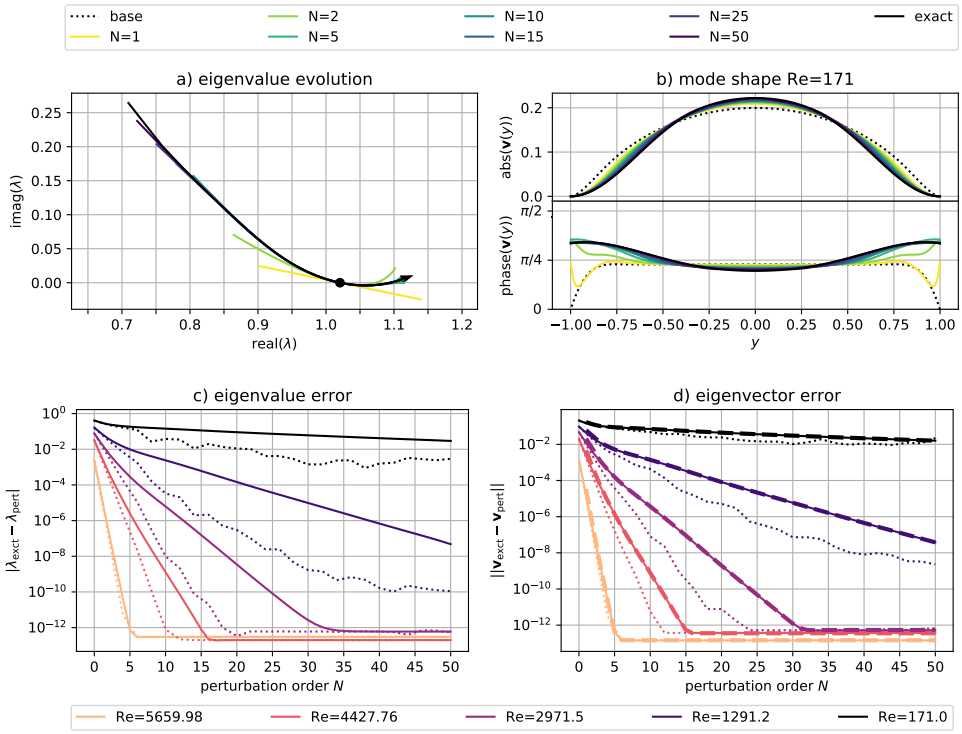

Figure 2: a) Eigenvalue trajectory when the Reynolds number is varied between Re = 5772±5601. The arrowhead indicates the direction of increasing Re. The black dot denotes the base eigenvalue at $\varepsilon = 0$. b) Absolute value and phase of the mode shape for Re = 171. The colored lines indicate the approximations obtained from various perturbation orders, while the black solid line denotes the exact mode shape. The black dashed line indicates the unperturbed mode shape at Re = Re_0. For the present example, already the first order approximation results in a reasonable prediction of the mode shape. c) Error between exact and estimated eigenvalue for various perturbation orders and Reynolds numbers. Solid lines represent power series while dotted lines indicate the error for diagonal Padé approximants obtained at even orders. d) error in the eigenvector estimate for the same set of parameters. Thick dashed lines correspond to the *a posteriori* method, while solid lines are obtained using the *a priori method*. Dotted lines represent results from the a priori method converted to diagonal Padé approximants.

The spatial stability problem is solved, in which a real oscillation frequency ω is prescribed, and wavenumber and growth rate of the spatial mode are computed as real and imaginary parts of the eigenvalue λ, respectively. The eigenvalue problem is non-normal, quartic in the eigenvalue, and linear in its parameters Re and ω. The problem has been extensively investigated in the

literature, see e.g. [38, 41]. The discretization is the same as that presented in [1], i.e. a Chebyshev collocation method using 64 points. The discretized operator takes the form

$$\begin{aligned}\mathbf{L}(\lambda, \mathrm{Re}) =& \lambda^4 \mathbf{I} + \mathrm{i}\lambda^3 \mathrm{Re}\mathbf{U} - 2\lambda^2 \mathbf{D}_2 - \mathrm{i}\lambda^2 \omega \mathrm{Re}\mathbf{I} \\ & - \mathrm{i}\lambda \mathrm{Re}\left(\mathbf{U}\mathbf{D}_2 + 2\mathbf{I}\right) + \mathrm{i}\omega \mathrm{Re}\mathbf{D}_2 + \mathbf{D}_4, \end{aligned} \tag{48}$$

where $\mathbf{I}$ is the identity matrix, $\mathbf{D}_2$ and $\mathbf{D}_4$ denote the discretization of the second and fourth order derivative operators, respectively, and $\mathbf{U}$ is the discretization matrix of the mean flow field. The discretized inner product amounts to the standard inner product $\langle \boldsymbol{a} | \boldsymbol{b} \rangle = \boldsymbol{a}^{\mathrm{H}} \boldsymbol{b}$.

In order to compare the results with those in the literature, the values of the frequency and the Reynolds number are fixed to $\omega_0 = 0.26943$ and $\mathrm{Re}_0 = 5772$, respectively. A neutrally stable eigenvalue exists for this choice of parameters, see [41] for further details. Application of the computational procedure discussed in §3.3 yields a baseline eigensolution corresponding to the eigenvalue $\lambda_0 = 1.02056 + 9.7 \times 10^{-7}\mathrm{i}$, which agrees with that reported in [1]. This baseline solution is fed to the perturbation algorithm, using as a perturbation parameter a variation in the Reynolds number, $\varepsilon := \mathrm{Re} - \mathrm{Re}_0$.

Figure 2a) shows the trajectory of the eigenvalue λ in the complex plane when the Reynolds number is varied between $\mathrm{Re} = 5772 \pm 5601$, as predicted by perturbation theory at various orders. The eigenvalue is more sensitive to variations in the Reynolds number when the latter is decreased rather than when it is increased, as the tail ($\mathrm{Re} = 171$) is farther away from the unperturbed solution than the head of the arrow ($\mathrm{Re} = 11373$). This emphasizes that the dependence of λ on Re is nonlinear. Figure 2a) also shows that the higher the order of the perturbation expansion, the better are the estimates for the eigenvalue. However, for large variations of the Reynolds number, the error on the eigenvalue remains large – note the distance between the tails of the eigenvalue trajectories of the exact and 50th-order approximation. This is because the power series expansion has reached the limit of its range of convergence. Indeed, it can be shown that, for any power series approximation the convergence rate – of both the estimated eigenvalue and the estimated eigenvector – decreases the stronger the perturbation parameter deviates from the unperturbed value. The series does not converge for values of $|\varepsilon|$ above a critical value δ, the radius of convergence. Focusing on the eigenvalue, the radius of convergence can be calculated from the expansion coefficients themselves as $\delta := \lim_{k\to\infty} |\lambda_k / \lambda_{k+1}|$,

provided that this limit exists. Figure 3 shows the first 50 terms of the sequence $\delta_k := |\lambda_k/\lambda_{k+1}|$, containing the ratio of two consecutive coefficients of the power series, which tends to the radius of convergence for large k. This estimate approaches the value of $\mathrm{Re}_0 = 5772$. Indeed, at $\mathrm{Re} = 0$ the Orr–Sommerfeld equation reduces to $\left(\frac{\mathrm{d}^2}{\mathrm{d}y^2} - \lambda^2\right)^2 v = 0$, which is a defective operator[6], as can be seen from the second and fourth terms of its general solution $v(y) = C_1 e^{-\lambda y} + C_2 y e^{-\lambda y} + C_3 e^{\lambda y} + C_4 y e^{\lambda y}$. The problem is therefore defective at $\mathrm{Re} = 0$, which limits the radius of convergence.

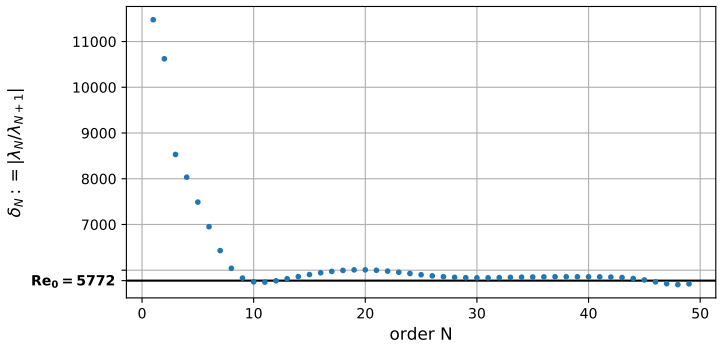

Figure 3: Radius of convergence δ as estimated from the coefficients of the eigenvalue power series predicted by perturbation theory. As expected, the convergence of the power series is limited by the singularity at $\mathrm{Re} = 0$, so that $\delta = \mathrm{Re}_0$.

Figure 2b) shows the unperturbed eigenfunction for $\mathrm{Re} = \mathrm{Re}_0$, corresponding to the baseline solution. In addition, the eigenfunction at $\mathrm{Re} = 171$ is shown, obtained from either perturbation theory estimates at various orders or solving directly the nonlinear eigenvalue problem. This plot demonstrates how the mode shape obtained from perturbation theory becomes an increasingly better approximation of the exact solution as the perturbation order is increased.

The convergence properties of the method are further illustrated in Figs. 2c) and 2d). The errors of the eigenvalue and eigenvector estimates obtained from perturbation theory are shown as a function of the perturbation order for various Reynolds numbers. A common technique to improve the con-

[6]Also, note that given the boundary conditions $v(\pm 1) = v'(\pm 1) = 0$, the differential equation does not have non-trivial solutions $v \neq 0$.

vergence properties is to convert the series into Padé approximants (see e.g. [27]). This consists in finding a rational function that features the same asymptotic behavior as the power series expansion at the expansion point:

$$\lambda(\varepsilon) \approx \sum_{n=0}^{N} \lambda_n \varepsilon^n \approx \frac{\sum_{l=0}^{L} a_l \varepsilon^l}{1 + \sum_{m=1}^{M} b_m \varepsilon^m}. \tag{49}$$

Given the first $N+1$ coefficients of the power series, $L+M+1 = N+1$ degrees of freedom (the coefficients a_l and b_m) in the Padé approximant can be determined. The coefficients are found by multiplying eq. (49) by the polynomial at the denominator of the r.h.s., sorting by like powers of ε, and solving the arising linear system of equations. In this study we focus on diagonal Padé approximants, i.e. approximants for which the polynomial degree of the numerator and of the denominator are equal ($L = M$). Note that, because $L+M = N$, these approximants are only defined for even perturbation orders N. In general, the numerical cost for the conversion from power series to Padé approximants is the solution of an $(N+1) \times (N+1)$ linear system. For scalar quantities, this is negligible w.r.t. the numerical costs of obtaining the N power series coefficients. For instance, using our implementation of the theory, solving the discretized Orr-Sommerfeld equation to find the baseline solution takes 0.2 s; computing the coefficients of the power series up to 10th, 30th, and 50th order – including an a priori normalization – takes 0.3, 7.9, and 387.8 s respectively[7]; converting the 50th order power series coefficients of the eigenvalue expansion into a diagonal Padé approximant takes 1 ms. Evaluation of the power series for the eigenvalue at 50th order for one specific Reynolds number took about 5 μs using Horner's scheme. The evaluation time of the power series for the eigenvector scales accordingly with the problem dimension of 64. As shown in Fig. 2c), the Padé approximants feature a smaller error than the power series approximations, and converge faster towards the exact solution.

Figure 2d) displays the errors between exact and estimated eigenvectors obtained using (i) the *a posteriori* normalization on the power series

[7] All reported times are wallclock times obtained at a Thinkpad Yoga 12 with an Intel Core i7-5500U CPU at 2.4 GHz operated with Ubuntu 18.04.02 LTS using Julia 1.1.0.

expansion (dashed lines); (ii) the *a priori* normalization on the power series expansion (solid lines); (iii) Padé approximations on each coefficients of the eigenfunctions (dotted lines). Despite minor differences, the first two methods exhibit the same convergence properties. At $\mathrm{Re} = 171$ the rate of convergence is slow; only little improvement is gained by increasing the perturbation order. This is because this value is approximately $\mathrm{Re}_0 - \delta$, i.e., it lies at the edge of the domain of convergence. Also, the error saturates due to machine precision, after having decreased by about 11 orders of magnitude. As for the eigenvalues, additional conversion of the power series to diagonal Padé approximants yields a quicker drop in the error with the perturbation order.

4.2. Biharmonic equation

This section considers the 2-dimensional biharmonic equation. The biharmonic operator naturally arises when modeling the vibration of a membrane [42]. For this example, a perturbation term proportional to an arbitrary parameter ε has been included in the equation. This could, for example, represent a non-homogeneous property of the membrane. The eigenvalue problem reads

$$\left(\nabla^4 + \varepsilon \cos(2\pi x)\cos(\pi y)\right) v = \lambda v \qquad \text{in } \Omega \tag{50a}$$

$$v = \nabla^2 v = 0 \qquad \text{on } \partial\Omega. \tag{50b}$$

In physical applications, the eigenvalue may be defined as the square of the angular frequency, $\lambda := \omega^2$. The eigenvalue problem is real, self-adjoint, and linear in both the eigenvalue λ and the perturbation parameter ε. Because the problem is self-adjoint, all eigenvalues are real. The domain has been set to $\Omega = (0, 2) \times (0, 1 + \sqrt{5})$. This choice makes the aspect ratio of the domain irrational and avoids the occurrence of accidental degenerate eigenvalues, which would require further care. Again, a Chebyshev collocation method is used to discretize the problem. The method uses 32 collocation points for each dimension. Consequently, the discrete operator is a dense 1024×1024-matrix, and reads

$$\mathbf{L}(\lambda, \varepsilon) := \mathbf{D}^4 + \varepsilon \mathbf{P} - \lambda \mathbf{I}, \tag{51}$$

where $\mathbf{P}$ is the matrix discretization of the spatially dependent perturbation, $\cos(2\pi x)\cos(\pi y)$. Again the discretized inner product amounts to the standard inner product $\langle \boldsymbol{a} | \boldsymbol{b} \rangle = \boldsymbol{a}^{\mathrm{H}} \boldsymbol{b}$.

For the unperturbed problem, obtained by fixing $\varepsilon = 0$, analytic expressions for the eigenvalues and eigenvectors can be found. For the present geometry they are

$$\lambda_{n,m} = \pi^4 \left(n^2 + \left(\frac{1+\sqrt{5}}{2} \right)^2 m^2 \right)^2 , \qquad v_{n,m}(x,y) = \sin(n\pi x) \sin(m\pi y) . \tag{52}$$

By numerically evaluating the smallest eigenvalue of (51) for $\varepsilon = 0$, we obtain $\lambda_0 \approx 1275.10$, which is consistent with the theoretical value for $\lambda_{1,1}$. In the next step the perturbation algorithm is applied to this eigenproblem, considering a power series expansion to 50th order and its conversion into a Padé approximant.

Figure 4a) compares the trajectory of the eigenvalue λ as a function of ε. It also indicates that the radius of convergence for the eigenvalue power series is $\delta \approx 12 \times 10^3$. Figure 4b) shows the unperturbed eigenfunction and perturbed ones corresponding to $\varepsilon = 10.73 \times 10^3$. For the perturbed case, various approximation orders and the exact solution are compared. The perturbation strongly affects the structure of the eigenfunction, but the power series expansion captures this effect well. As the perturbation parameter is within the radius of convergence, the approximation improves with higher perturbation order.

Figure 4c) shows the error evolution of the eigenvalue λ when the perturbation order is increased, for various values of the perturbation parameter ε. The error does not evolve in a smooth manner. A similar trend can be observed in the error of the Taylor series expansion of, for example, $\cos(x)$ at $x = 0$; the error decreases at even expansion orders and remains constant at odd expansion orders. It is indeed not necessary for a power series to reduce the approximation error order by order even within the radius of convergence. It simply converges to the solution for high expansion orders, which is what Fig. 4c) shows for $\varepsilon \lesssim 12 \times 10^3$. The error saturates due to machine precision after decreasing by about 11 orders of magnitude. Note that conversion to diagonal Padé approximants significantly improves the convergence property. For $\varepsilon = 14500$ the Padé approximant converges even though the original power series was clearly divergent. Analogous results can be seen in Fig. 4d) for the eigenvector error when using the *a posteriori* normalization method. In contrast, the *a priori* procedure yields smoother convergence. This might be attributed to the fact that in the former the eigenvalue approximations

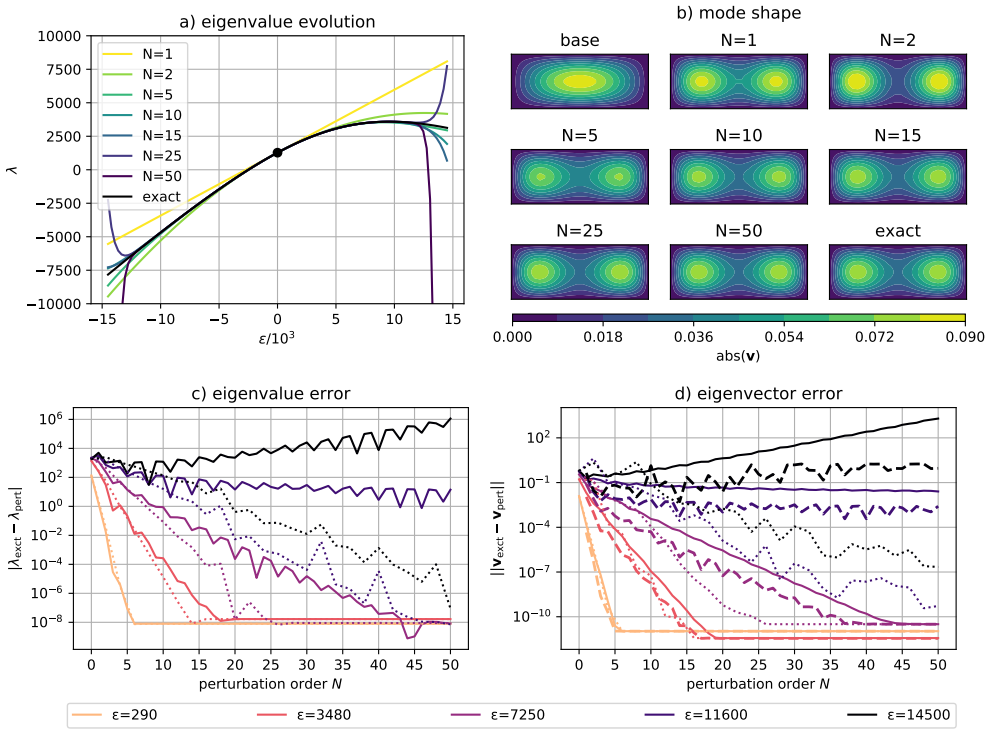

Figure 4: a) Eigenvalue λ of the perturbed biharmonic equation as a function of the perturbation parameter ε. b) Unperturbed (base) eigenfunction for $\varepsilon = 0$ and eigenfunctions for $\varepsilon = 10.73 \times 10^3$, obtained from either perturbation theory and by numerically solving the perturbed eigenproblem. Note that the axes are not equally scaled. c) Error between exact and estimated eigenvalue for various perturbation orders and parameter variations. The solid lines represents power series results while the dotted line indicate diagonal Padé approximants. d) Error between exact and estimated eigenvectors for various perturbation orders and parameter variations. Solid and dashed lines indicate power series results obtained with the *a priori* and *a posteriori* approach, respectively. The dotted line represents results found when converting the a-priori normalized results to diagonal Padé approximants.

are explicitly used to calculate the coefficients $c(\varepsilon)$ [eq. (35)], whereas in the latter, the coefficients c_k explicitly depend on the eigenvectors only [eq. (32)]. Nonetheless, for high perturbation orders the, two methods yield analogous rates of convergence when using power series and conversion to diagonal Padé approximants clearly accelerates the convergence.

4.3. Thermoacoustic Helmholtz equation

In the last example, the thermoacoustic Helmholtz equation as a model for a Rijke tube is considered. Rijke-tube configurations are frequently used as models for thermoacoustic systems, for example, in [43, 44, 45, 26]. The model equation reads

$$\nabla \cdot \left(c^2 \nabla \hat{p}\right) + \omega^2 \hat{p} = \frac{A}{V}\left(c_b^2 - c_u^2\right) n e^{-\mathrm{i}\omega\tau}\, \nabla \hat{p}|_{\boldsymbol{x}_{\mathrm{ref}}} \cdot \boldsymbol{n}_{\mathrm{ref}}. \tag{53}$$

Equation (53) models acoustic oscillations coupled to a time-delayed source, where the latter is, in turn, driven by the acoustic field at a reference position. The equation is obtained by introducing the ansatz $p(\boldsymbol{x}, t) = \hat{p}(\boldsymbol{x}) e^{\mathrm{i}\omega t}$ into a corresponding wave equation. Consequently, the eigenvalue ω describes frequency and growth rate of an associated pressure fluctuation mode $\hat{p}(\boldsymbol{x})$. The left hand side of the equation models acoustic wave propagation, with c denoting the spatial distribution of the speed of sound. The right hand side originates from an unsteady heat release rate term. It is expressed by the so-called n–τ model, which represents the linear response of the heat release rate fluctuations with respect to acoustic velocity fluctuations at a reference position x_{ref}, located just upstream of the heat source [46]. τ denotes the time delay and n the coupling strength between the acoustic velocity fluctuation and the heat release rate. In this example, $n = 1$ in the domain of heat release – a thin region located in the middle of the tube with a length of 0.1 mm and with the same cross-sectional area A of the tube – and $n = 0$ elsewhere. Across the domain of heat release, the temperature increases due to the heat addition; c_b and c_u denote burnt and unburnt gas temperature, respectively. Length and diameter of the tube are set to $L = 0.5\,\mathrm{m}$ and $D = 0.05\,\mathrm{m}$. Moreover, sound hard ($\nabla p \cdot \boldsymbol{n} = 0$) and sound soft ($p = 0$) boundary conditions are set at the inlet and the outlet of the tube, respectively. The speed of sound in the unburnt and burnt regions is set to $c_{\mathrm{u}} = 348\,\mathrm{m/s}$ and $c_{\mathrm{u}} = 696\,\mathrm{m/s}$, respectively.

Perturbations in the time delay parameter τ are considered. The time delay is, therefore, split into the baseline value τ_0 and the perturbation parameter $\varepsilon = \Delta\tau := \tau - \tau_0$. The problem is discretized with a Bubnov–Galerkin finite element method using linear tetrahedral Lagrange elements. The discretized eigenproblem features 730 degrees of freedom, and reads

$$\mathbf{L}(\omega, \tau)\boldsymbol{v} := \left[\mathbf{K} + \omega\mathbf{C} + \omega^2\mathbf{M} + e^{-\mathrm{i}\omega(\tau_0+\Delta\tau)}\mathbf{Q}\right]\boldsymbol{v} = 0, \tag{54}$$

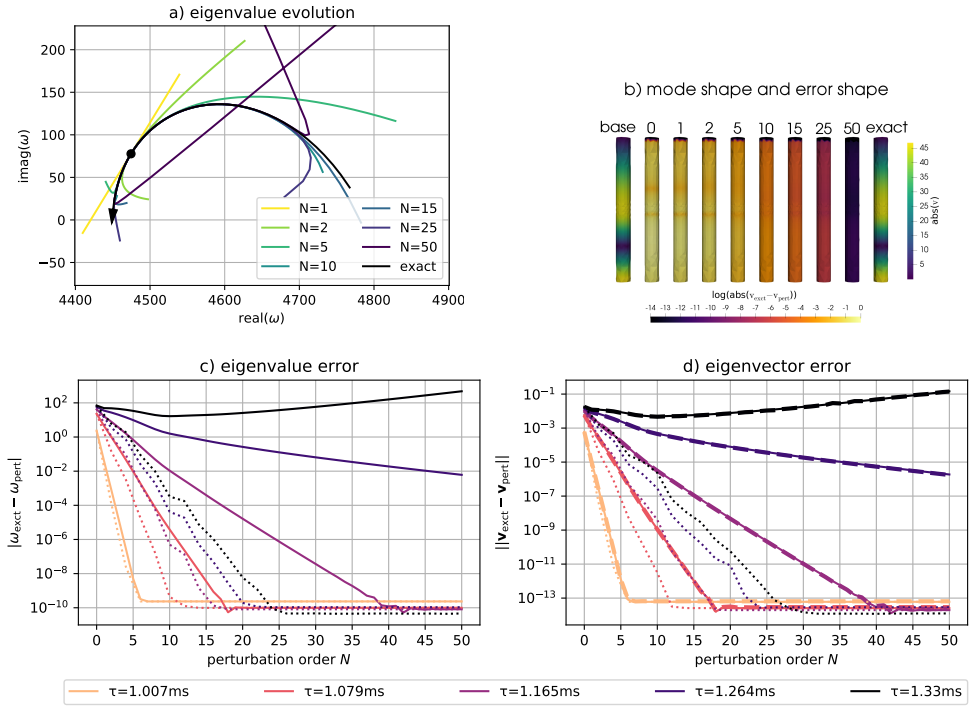

Figure 5: a) Eigenvalue trajectory when the time delay is varied between $\tau = 1.000\,\text{ms} \pm 0.33\,\text{ms}$; the arrowhead indicates the direction of increasing τ. The black dot denotes the base eigenvalue. Note, that the divergence of the 50th order approximation is so strong that the ends of the trajectory are not shown. b) Absolute value of the eigenfunction for the baseline setting and a value of $\tau = 1.295\,\text{ms}$ and error of approximations computed by either perturbation theory of various orders. c) Error between exact and estimated eigenvalue for various perturbation orders and time delays numbers. Power series approximations are highlighted by a solid line, the dotted line indicates diagonal Padé approximants. d) Error between exact and estimated eigenvectors for various perturbation orders and time delays. Power series approximants obtained with solid line highlights the a priori method while the dashed line indicates results obtained from the a posteriori approach. In the present case, the a posteriori method yields slightly better results.

where $\mathbf{K}$ is the stiffness matrix arising from the discretization of $\nabla \cdot c^2 \nabla$, $\mathbf{C}$ the damping matrix originating from the boundary conditions, $\mathbf{M}$ the mass matrix representing the discretized identity operator, $\mathbf{Q}$ the discretization matrix accounting for the heat release, and $\boldsymbol{v}$ is the eigenvector, containing the values of the pressure at the mesh nodes. With this discretization the discretized inner product that is used to normalize the modes amounts to $\langle \boldsymbol{a} | \boldsymbol{b} \rangle = \boldsymbol{a}^{\mathrm{H}} \mathbf{M} \boldsymbol{b}$.The eigenvalue problem (54) is non-normal and, due to the

time-lag term, highly nonlinear in both the eigenvalue ω and the parameter τ. The unperturbed eigenproblem ($\Delta\tau = 0$) features an eigenvalue $\omega_0 \approx 4475 + 78\mathrm{i}\,\mathrm{s}^{-1}$. In conjunction with the corresponding direct and adjoint eigenvectors, this baseline solution is fed to the perturbation algorithm. The calculation of the power series coefficients for the eigenvalues and eigenvectors is performed up to 50th order. The power series coefficients are used to calculate the coefficients of diagonal Padé approximants.

Figure 5a) shows the trajectory of the eigenvalue ω when the time delay is varied between $\Delta\tau = \pm 0.330\,\mathrm{ms}$. This variation exceeds the radius of convergence, which is $\delta = 0.0295\,\mathrm{ms}$ as estimated from the coefficients of the eigenvalue power series. Hence, the estimates obtained from perturbation theory diverge from the exact solution at the ends of the shown trajectory; they converge to the exact solution otherwise. Note that for a decrease in τ the imaginary part of the eigenvalue decreases again after moderately increasing before. This means the mode destabilizes. This effect is not accurately captured by low-order theory, yet by the higher-order approximations. Figure 5b)shows the absolute value of the base-line mode shape (leftmost) and the perturbed mode shape at $\Delta\tau = 0.191\,\mathrm{ms}$ (rightmost). Additionally, it compares the absolute value of the error of the eigenfunctions as obtained from perturbation theory of various orders. It is obvious how the error decreases with an increasing perturbation order.

Figure 5c) and d) further illustrate the convergence properties of the method. The error of eigenvalue and eigenfunction approximations is shown for various values of τ. The eigenvector error is shown for the results obtained using the *a priori* (solid) and the *a posteriori* (dashed) normalization schemes for the power series expansions. They show the same convergence properties for this case. For a time delay $\tau = 1.330\,\mathrm{ms}$, the error in both the eigenvalue and the eigenvector increases at high perturbation orders; this parameter value lies outside the radius of convergence. For smaller values of τ, the power expansions for both eigenvalue and eigenvector converge, and are limited by machine precision. Again, conversion to diagonal Padé approximants improves the convergence rate of eigenvalues and eigenvectors (dotted lines). Furthermore, even for $\tau = 1.330\,\mathrm{ms}$, which lies outside of the convergence radius of the power series, a convergent Padé approximant is obtained.

5. Conclusions

A high-order, adjoint-based theory for the calculation of power series coefficients of simple eigenvalues and their associated eigenfunctions, arising from the perturbation of (generally) nonlinear and non-self-adjoint eigenproblems, was discussed. Two different normalization methods for the estimation of the corresponding eigenfunctions were compared. The derived explicit, incremental formulas and the proposed numerical algorithm are independent of the considered eigenvalue problem and highly parallelizable.

The three applications examples discussed demonstrate the broad applicability of the theory. They encompassed eigenvalue problems that (i) depend linearly, polynomially, and exponentially on the eigenvalue; (ii) are represented by both self-adjoint and non-self-adjoint operators; and (iii) describe one-, two-, and three-dimensional eigenproblems arising in different scientific fields. Both eigenvalues and eigenvectors of the considered examples converged to the exact solution within the radius of convergence of the power series. More specifically, the convergence rate of the eigenvectors was shown to be independent from the normalization method chosen. As expected from the asymptotic behavior of power series expansions, the smaller the considered perturbation in the parameter the less terms are needed to have an accurate approximation. Moreover, the accuracy of the estimates can be improved when converting the power series to Padé approximants, which also have a larger domain of convergence than the power series approximations.

Whether the perturbation method is more efficient than repeatedly solving the eigenvalue problem cannot be said *per se*. This depends on the relevant parameter range for which the eigensolutions are needed, on the number of data points to be evaluated in this range, on the required accuracy, and on the capacity of the available hardware for parallelization. Nonetheless, besides the possible reduction of computational costs, there are more advantages of large-order perturbation theory. First, as it makes the dependence of the eigenvalue on the parameter explicit, derivatives of ω with respect to the parameter that go beyond first-order sensitivity are directly accessible, unveiling the nonlinear dependency of the eigenvalues on the parameters of interest. As the expansion is asymptotic, it can also be used to estimate the truncation error when truncating the series at lower order. Second, on top of allowing a quick estimation of the eigenvalues in a given region in parameter space, the presented theory can also be used to accelerate the performance of existing nonlinear eigenvalue solvers. For example, using the eigenvalue

approximations obtained at low perturbation order (say 5th), good guesses can be fed to, e.g., the Rayleigh quotient iterative method. Starting from a good guess guarantees the convergence of the algorithm towards a close-by solution, and greatly reduces the number of iterations required by the algorithm to converge towards it.

Acknowledgements

Alessandro Orchini thanks the Alexander von Humboldt Foundation for financial support through the Humboldt Research Fellowship for Postdoctoral Researchers. The authors also thank Philip E. Buschmann and Jakob G. R. von Saldern for their help with the implementation of the software code.

References

[1] T. Betcke, N. J. Higham, V. Mehrmann, C. Schröder, F. Tisseur, NLEVP: A collection of nonlinear eigenvalue problems, ACM Trans. Math. Softw. 39 (2013) 7:1–7:28. doi:10.1145/2427023.2427024.

[2] L. N. Trefethen, M. Embree, Spectra and Pseudospectra: The Behavior of Nonnormal Matrices and Operators, Princeton University Press, 2005. URL https://press.princeton.edu/titles/8113.html

[3] J. López-Gómez, C. Mora-Corral, Algebraic Multiplicity of Eigenvalues of Linear Operators, Vol. 177 of Operator Theory: Advances and Applications, Birkhäuser, 2007. doi:10.1007/978-3-7643-8401-2.

[4] L. Rayleigh, The Theory of Sound, Dover Publications, 1945. doi:10.1017/CBO9781139058087.

[5] E. Schrödinger, Quantisierung als Eigenwertproblem [quantization as an eigenvalue problem], Annalen der Physik 385 (1926) 437–490. doi:10.1002/andp.19263840404.

[6] E. Fues, Das Eigenschwingungsspektrum zweiatomiger Moleküle in der Undulationsmechanik [the spectrum of eigenoscillations of diatomic molecules in undulatory mechanics], Annalen der Physik 385 (1926) 367–396. doi:10.1002/andp.19263851204.

[7] S. Gorgizadeh, T. Flisgen, U. van Rienen, Eigenmode computation of cavities with perturbed geometry using matrix perturbation methods applied on generalized eigenvalue problems, Journal of Computational Physics 364 (2018) 347 – 364. doi:10.1016/j.jcp.2018.03.012.

[8] T. Kato, Perturbation Theory for Linear Operators, Vol. 132 of Grundlehren der mathematischen Wissenchaften, Springer-Verlag, 1980. doi:10.1007/978-3-642-66282-9.

[9] P. Sirković, D. Kressner, Subspace acceleration for large-scale parameter-dependent hermitian eigenproblems, SIAM Journal on Matrix Analysis and Applications 37 (2) (2016) 695–718. doi:10.1137/15M1017181.

[10] C. Buth, R. Santra, L. Cederbaum, Non-Hermitian Rayleigh–Schrödinger perturbation theory, Physical Review A 69 (2004) 032505. doi:10.1103/PhysRevA.69.032505.

[11] A. Bottaro, P. Corbett, P. Luchini, The effect of base flow variation on flow stability, Journal of Fluid Mechanics 476 (2003) 293–302. doi:10.1017/S002211200200318X.

[12] O. Marquet, D. Sipp, L. Jacquin, Sensitivity analysis and passive control of cylinder flow, Journal of Fluid Mechanics 615 (2008) 221–252. doi:10.1017/S0022112008003662.

[13] O. Tammisola, F. Giannetti, V. Citro, M. P. Juniper, Second-order perturbation of global modes and implications for spanwise wavy actuation, Journal of Fluid Mechanics 755 (2014) 314–335. doi:10.1017/jfm.2014.415.

[14] C. Mettot, F. Renac, D. Sipp, Computation of eigenvalue sensitivity to base flow modifications in a discrete framework: Application to open-loop control, Journal of Computational Physics 269 (2014) 234 – 258. doi:10.1016/j.jcp.2014.03.022.

[15] L. Magri, M. P. Juniper, Sensitivity analysis of a time-delayed thermo-acoustic system via an adjoint-based approach, Journal of Fluid Mechanics 719 (2013) 183–202. doi:10.1017/jfm.2012.639.

[16] G. A. Mensah, J. P. Moeck, Acoustic damper placement and tuning for annular combustors: an adjoint-based optimization study, Journal of Engineering for Gas Turbines and Power 139 (2017) 061501. doi:10.1115/1.4035201.

[17] V. Mehrmann, H. Voss, Nonlinear eigenvalue problems: a challenge for modern eigenvalue methods, GAMM-Mitteilungen 27 (2004) 121–152. doi:10.1002/gamm.201490007.

[18] S. Güttel, F. Tisseur, The nonlinear eigenvalue problem, Acta Numerica 26 (2017) 1–94. doi:10.1017/S0962492917000034.

[19] M. S. Jankovic, Exact nth derivatives of eigenvalues and eigenvectors, Journal of Guidance, Control, and Dynamics 17 (1) (1994) 136–144. doi:10.2514/3.21170.

[20] A. L. Andrew, K.-W. E. Chu, P. Lancaster, Derivatives of eigenvalues and eigenvectors of matrix functions, SIAM Journal on Matrix Analysis and Applications 14 (4) (1993) 903–926. doi:10.1137/0614061.

[21] P. Lancaster, A. S. Markus, F. Zhou, Perturbation theory for analytic matrix functions: The semisimple case, SIAM Journal on Matrix Analysis and Applications 25 (2003) 606–626. doi:10.1137/S0895479803423792.

[22] W. Michiels, I. Boussaada, S.-I. Niculescu, An explicit formula for the splitting of multiple eigenvalues for nonlinear eigenvalue problems and connections with the linearization for the delay eigenvalue problem, SIAM Journal on Matrix Analysis and Applications 38 (2017) 599–620. doi:10.1137/16M107774X.

[23] O. N. Kirillov, Nonconservative Stability Problems of Modern Physics, Vol. 14 of De Gruyter Studies in Mathematical Physics, de Gruyter, 2013.
URL https://www.degruyter.com/view/product/179816

[24] F. M. Fernández, Introduction to Perturbation Theory in Quantum Mechanics, 1st Edition, CRC Press, 2000.
URL https://www.crcpress.com/9780849318771

[25] D. Klindworth, K. Schmidt, An efficient calculation of photonic crystal band structures using Taylor expansions, Communications in Computational Physics 16 (2014) 1355–1388. doi:10.4208/cicp.240513.260614a.

[26] G. A. Mensah, L. Magri, J. P. Moeck, Methods for the calculation of thermoacoustic stability boundaries and Monte Carlo-free uncertainty quantification, Journal of Engineering for Gas Turbines and Power 140 (6) (2018) 061501. doi:10.1115/1.4038156.

[27] W. Paulsen, Asymptotic Analysis and Perturbation Theory, Chapman and Hall/CRC, 2013.
URL https://www.crcpress.com/9781466515116

[28] P. D. Miller, Applied Asymptotic Analysis, Vol. 75 of Graduate Studies in Mathematics, American Mathematical Society, 2006. doi:10.1090/gsm/075.

[29] R. G. Parker, C. D. J. Mote, Exact boundary condition perturbation solutions in eigenvalue problems, ASME Journal of Applied Mechanics 63 (1996) 128–135. doi:10.1115/1.2787187.

[30] P. Luchini, A. Bottaro, Adjoint equations in stability analysis, Annual Review of Fluid Mechanics 46 (2014) 493–517. doi:10.1146/annurev-fluid-010313-141253.

[31] M. Giles, J. Duta, M.C. Mueller, N. Pierce, Algorithm developments for discrete adjoint methods, AIAA Journal 41 (2003) 198–205. doi:10.2514/2.1961.

[32] P. Lancaster, A generalised Rayleigh quotient iteration for lambda-matrices, Archive for Rational Mechanics and Analysis 8 (1961) 309–322. doi:10.1007/BF00277446.

[33] A. S. Householder, The Numerical Treatment of a Single Nonlinear Equation, McGraw-Hill, New York, 1970, isbn: 0070304653.

[34] W.-J. Beyn, An integral method for solving nonlinear eigenvalue problems, Linear Algebra and its Applications 436 (2012) 3839–3863.

[35] P. E. Buschmann, G. A. Mensah, F. Nicoud, J. P. Moeck, Solution of thermoacoustic eigenvalue problems with a non-iterative method, in: ASME Turbo Expo, 2019, pp. GT2019–90834 (15 pages).

[36] L. Bracci, L. E. Picasso, A simple iterative method to write the terms of any order of perturbation theory in quantum mechanics, The European Physical Journal Plus 127 (2012). doi:10.1140/epjp/i2012-12119-6.

[37] J. Kelleher, Encoding partitions as ascending compositions, Ph.D. thesis, Department of Computer Science University College Cork (December 2005).
URL http://jeromekelleher.net/downloads/k06.pdf

[38] P. J. Schmid, D. S. Henningson, Stability and Transition in Shear Flows, Springer, 2000. doi:10.1007/978-1-4613-0185-1.

[39] M. J. Kingan, Aeroacoustic noise produced by an aerofoil, Ph.D. thesis, University of Canterbury, Christchurch, New Zealand (2005).

[40] T. P. Chong, P. Joseph, "ladder" structure in tonal noise generated by laminar flow around an airfoil, The Journal of the Acoustical Society of America 131 (6) (2012) EL461–EL467. doi:10.1121/1.4710952.

[41] F. Tisseur, N. J. Higham, Structured pseudospectra for polynomial eigenvalue problems, with applications, SIAM Journal on Matrix Analysis and Applications 23 (1) (2001) 187–208. doi:10.1137/S0895479800371451.

[42] A. E. Love, The small free vibrations and deformation of a thin elastic shell, Philosophical Transactions of the Royal Society of London A: Mathematical, Physical and Engineering Sciences 179 (1888) 491–546. doi:10.1098/rsta.1888.0016.

[43] A. P. Dowling, The calculation of thermoacoustic oscillations, Journal of Sound and Vibration 180 (1995) 557–581. doi:10.1006/jsvi.1995.0100.

[44] F. Nicoud, L. Benoit, C. Sensiau, T. Poinsot, Acoustic modes in combustors with complex impedances and multidimensional active flames, AIAA Journal 45 (2007) 426–441. doi:10.2514/1.24933.

[45] A. Orchini, S. J. Illingworth, M. P. Juniper, Frequency domain and time domain analysis of thermoacoustic oscillations with wave-based acoustics, Journal of Fluid Mechanics 814 (2014) 570–591. doi:10.1017/jfm.2017.32.

[46] L. Crocco, Theoretical studies on liquid-propellant rocket instability, in: The Combustion Institute: Tenth Symposium (International) on Combustion, 1965, pp. 1101–1128. doi:10.1016/S0082-0784(65)80249-1.